PHYSICAL REVIEW LETTERS

Origins of Nanoscale Heterogeneity in Ultrathin Films

J. B. Hannon*

IBM Research Division, T. J. Watson Research Center, Yorktown Heights, New York 10598, USA

J. Sun and K. Pohl

Department of Physics, University of New Hampshire, Durham, New Hampshire 03824, USA

G. L. Kellogg

Sandia National Laboratories, Albuquerque, New Mexico 87185, USA

A key challenge in thin-film growth is controlling structure and composition at the atomic scale. We have used spatially resolved electron scattering to measure how the three-dimensional composition profile of an alloy film evolves with time at the nanometer length scale. We show that heterogeneity during the growth of Pd on Cu(001) arises naturally from a generic step-overgrowth mechanism relevant in many growth systems.

Thin films play a key role in many technologies. Applications range from promoting chemical reactions at surfaces, preventing interdiffusion, and electrical isolation to more exotic ones in nanotechnology, where reduced dimensionality gives rise to unique electronic or magnetic properties. One particularly important issue in the growth of ultrathin films is controlling compositional heterogeneity. It is well known that films can be inhomogeneous, but determining exactly *how* and *why* heterogeneity develops is extremely difficult. In general, understanding how the three-dimensional composition profile of the film evolves with time is required. Detailed information of this type has proven difficult to obtain because high spatial resolution must be combined with subsurface chemical sensitivity. Here we describe spatially resolved electron diffraction measurements that overcome these limitations and allow us to unambiguously determine how nanometer-scale compositional inhomogeneity develops during growth. By measuring the evolution of the three-dimensional composition of a growing film in real time, we show that a simple step-overgrowth mechanism, potentially relevant in many systems, is responsible for the heterogeneity we measure.

We have measured the development of compositional heterogeneity during the growth of ultrathin Pd films on Cu(001) using low-energy electron microscopy (LEEM) [1]. In LEEM, an image is formed from the low-energy electrons reflected from a surface. An image of the Cu(001) surface recorded during Pd deposition at 200 °C is shown in Fig. 1(a). The surface contains a number of single-atomic layer steps, identified by sharp changes in image contrast. In these regions, one sees dendritic-type growth outward from the advancing step and a continuous decrease in image intensity away from the step on the upper terrace. The image intensity is determined by the local electron reflectivity. While the spatial variation of the intensity shows directly that the surface is heterogeneous, the

exact nature of the inhomogeneity is unclear. One would like to understand precisely how the surface is inhomogeneous and to identify the atomic-scale kinetic processes that are responsible. These are difficult issues because of the inherent complexity of the growth environment.

Here we show how spatially resolved measurements of the alloy composition can be used to understand the heterogeneous growth. As we describe in detail below, we determine the alloy concentration point by point on the surface by quantitatively analyzing the image intensity as a
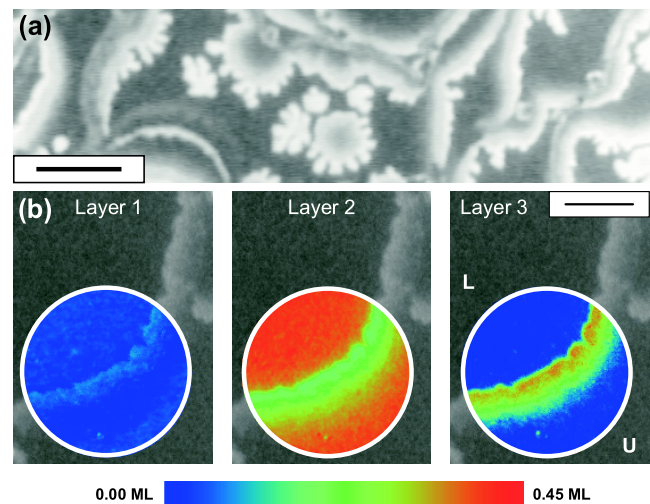

FIG. 1 (color online). (a) 13.1 eV LEEM image recorded after the deposition of ∼0.6 ML Pd on Cu(001) at 200 °C. Scale bar, 1 μm. (b) 3D map of the Pd concentration near a surface step. The color images (circled in white) show the concentrations in the first three surface layers after deposition of 0.45 ML of Pd at 200 °C. The spatial resolution is 8.5 nm. The colored maps are superimposed on the corresponding 13.1 eV gray-scale LEEM image. The upper (U) and lower (L) terraces are marked. Scale bar, 500 nm.

function of electron kinetic energy. The results of this analysis are shown in Fig. 1(b) for an area of the surface near an atomic step. The images show the concentration of Pd in each of the first three layers of the surface after the deposition of 0.45 ML of Pd at 200 °C. The analysis shows that the top layer is almost entirely Cu, while most of the deposited Pd is located in the second layer. Near the step, there are significant variations in the Pd concentration. Most importantly, there is a substantial amount of Pd in the *third* layer on the *upper* side of the step, while on the *lower* side there is virtually none in the third layer.

The presence of third-layer Pd exclusively at the upper side of the step suggests a possible mechanism driving the heterogeneity: alloying via step overgrowth. The principle is illustrated schematically in Fig. 2. The figure shows a side view of the surface near a step at 3 times $t_1 < t_2 < t_3$ during Pd deposition at 200 °C. We label the Pd concentrations in the first three surface layers c_1, c_2, and c_3. Motivated by the experimental results, we assume that there is no Pd in the first layer ($c_1 = 0$) and that Pd in the second layer (c_2) is spatially uniform (due to rapid surface diffusion). Furthermore, we assume that there is no direct migration of Pd to the third layer ($c_3 = 0$ far from the steps). As more Pd is deposited, the concentration of Pd in the second layer increases and the step moves to the right due to the attachment of ejected Cu atoms. Part of the surface is overgrown by the advancing step, effectively transferring Pd from the second layer (in front of the step) to the third layer (behind the step). The mobility of Pd in the third layer is presumably much lower than that of Pd in the second layer because the environment is "bulk-like." The activation energy for vacancy-mediated diffusion in *bulk* copper is 2.06 eV [2], while that for vacancy-mediated diffusion at the (001) *surface* is only 0.80 eV [3].
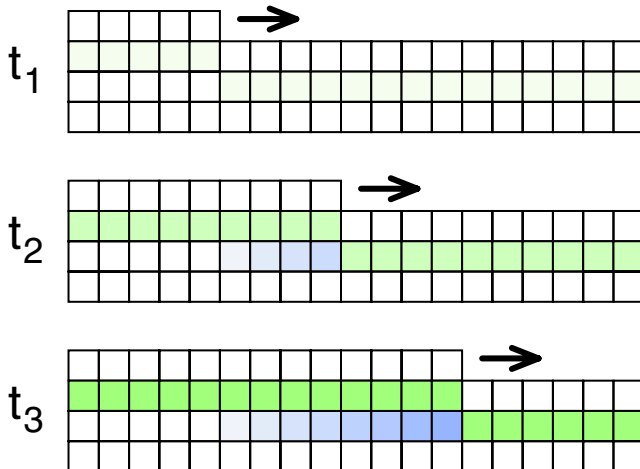
Pd transferred to the third layer is virtually immobile at 200 °C. In the simplest scenario, the amount of Pd buried by the step is equal to the instantaneous concentration in the second layer, leading to a *characteristic profile* for c_3 in the overgrown region.

Before evaluating the step-overgrowth model in more detail, we first describe how the layer-resolved Pd concentrations shown in Fig. 1(b) are derived from the image intensities. Our analysis is based on comparing the measured electron reflectivity to that calculated for a trial structure and is essentially identical to the approach used to analyze low-energy electron diffraction (LEED) [4]. The method is similar in spirit to the "fingerprinting" approach used by Schmid *et al.* to determine overlayer coverages during a chemical reaction [5]. In our experiments, the incident electron beam is normal to the surface. We place an aperture in the optical path so that only electrons reflected specularly—i.e., into the (00) LEED diffraction beam—contribute to the image. Thus, the LEEM image intensity measures the spatial variation of the (00) diffraction beam at a particular energy. By recording images at different electron beam energies, the dependence of the reflected electron intensity on electron kinetic energy is recorded for any point in the field of view. In the LEED literature, these data are called intensity-versus-voltage curves (or simply "*IV* curves"). The *IV* curves are computed for a trial structure and compared with experiment. The parameters of the trial structure (which include the Pd concentrations in the first three surface layers) are varied to give the best agreement with the measured *IV* curve. In this way, we determine the values of c_1, c_2, and c_3 point by point at the surface. Examples of measured and computed *IV* curves are shown in Fig. 3.

In our calculations, the alloy composition in the three outermost layers is optimized using the average *t*-matrix approximation method [6]. We find the best agreement between the measured and computed *IV* curves when the

FIG. 2 (color online).   A schematic of step-flow overgrowth. Side views of the Cu surface are shown at 3 times ($t_1 < t_2 < t_3$) during Pd deposition. The Pd composition in the second (third) layer is shown in green (blue). Step-flow overgrowth converts mobile Pd in the second layer into fixed Pd in the third layer.
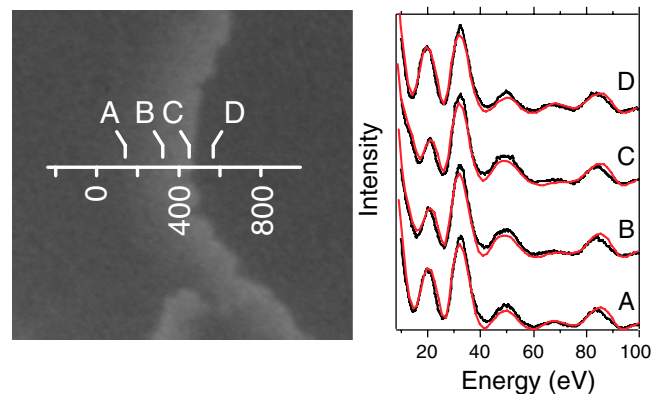
FIG. 3 (color online).   13.5 eV LEEM image recorded after the deposition of 0.45 ML of Pd at 200 °C. Distances along the line scan are given in nanometers. At the start of Pd deposition, the step was located at $x = 0$. Measured (computed) *IV* curves at *A*, *B*, *C*, and *D* are shown in black (red).

Pd in each layer is located primarily in one 2×2 sublattice, in agreement with previous LEED analysis [7]. One significant difference between conventional LEED and LEEM is that the electron energy in LEEM is typically much lower. At very low energies, inelastic damping is difficult to treat with the standard LEED-*IV* formalism because the electron mean free path depends strongly on the energy. Therefore, we use an energy-dependent optical potential (i.e., the imaginary part of inner potential) of the form $V_{im} = V_{damp}E^{1/3}$ [8], where E is the beam energy in eV and V_{damp} is a parameter to be optimized. The real part of inner potential is assumed constant at -13.4 eV below 36 eV and has an $E^{-1/2}$ dependence above 36 eV, as proposed by Rundgren [9]. The latter is particularly relevant for Cu(100), where the correct treatment of the low-energy electrons resolved a controversial claim of an in-plane contraction [10,11]. We find the best agreement between the calculated and measured *IV* curves with $V_{damp} = 0.86$ eV$^{2/3}$ and the real part of the inner potential fixed at -13.4 eV for $E < 36$ eV. Details of the LEED optimization process are described elsewhere [12].

We now describe how the alloy compositions measured near a step validate the step-overgrowth model. Three key signatures of the overgrowth model are (1) the asymmetry in the third-layer Pd concentration near a step, (2) the characteristic profile of the third-layer Pd in the overgrown region, and (3) the correlation between third-layer Pd behind the step and the second-layer Pd in front of the step. Each of these predictions can be rigorously tested by analyzing the Pd concentration near the step. *IV* curves from four points along a line crossing a step are shown in Fig. 3. The most significant differences between the curves occur for energies below 30 eV. In the overgrown region, the intensity of the peak near 20 eV is lower, and a low-energy shoulder is present at about 13 eV. We find very good agreement between the calculated and measured *IV* curves at all points on the surface.

The variation in c_1, c_2, and c_3 along a line crossing a step is shown Fig. 4(a). The analysis shows that most of the Pd is located in the second layer, in agreement with previous LEED studies [7]. Away from the step, the concentrations are spatially uniform, with $c_2 \approx 0.4$ and c_1 and c_3 about zero. Near the step, c_3 is large on the upper side of the step but drops dramatically to zero at the step position. The value of c_3 at the upper side of the step is equal to that of c_2 on the *lower* side of the step. This correlation strongly suggests that Pd in the third layer arrives there via the step-overgrowth process.

The time evolution of c_3 further confirms this picture. The variation in c_3 near the step is shown in Fig. 4(b) for three different times during Pd deposition. It is clear that the amount of Pd buried by the step increases monotonically with time as the step moves. If the buried Pd is immobile, the profile of c_3 in the overgrown region should not change with time. For example, the three curves shown
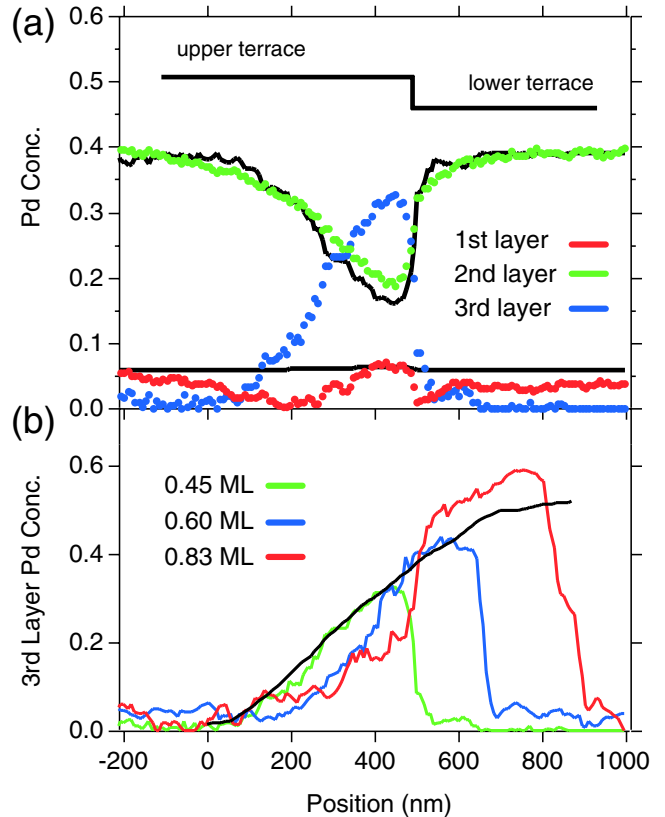

FIG. 4 (color online).   Pd concentration along the line indicated in Fig. 3. (a) Layer-resolved Pd concentrations measured for a total Pd coverage of 0.45 ML. (b) Third-layer Pd concentration measured at three different Pd coverages (i.e., deposition times) during deposition at 200 °C. During growth, the step advances to the right.

in Fig. 4(b) should agree for $x < 500$ nm, which they do. This suggests that diffusion into or out of the third layer is slow at 200 °C. The data in Fig. 4(a) suggest that the Pd instantaneously buried by the step is equal to the value of c_2 on the terrace. That is, the spatial profile of the buried Pd is related to the time profile of the Pd in the second layer. In other words, $c_3(x(t)) = c_2(t)$, where $x(t)$ is the step position. We have measured both $x(t)$ and $c_2(t)$ (far from the steps), which allows us to test this prediction. The black line in Fig. 4(b) shows the profile predicted by the step-overgrowth model. The agreement is quite good, showing that the spatial profile of the buried Pd $c_3(x)$ is directly related to the distribution of mobile Pd on the terrace $c_2(t)$. The direct comparison of the measured and predicted alloy composition profiles confirms the basic picture of compositional heterogeneity driven by step overgrowth.

We have shown that step overgrowth converts mobile, second-layer Pd into immobile Pd in the third layer. We now show how correlations between the amount of Pd in neighboring layers gives insight into the bonding and stability of the alloy film. As discussed above, the profile for c_3 in Fig. 4(a) is determined by the step-overgrowth

mechanism. Contrary to the assumptions of the simplified step-overgrowth model (Fig. 2), c_2 is *not* spatially uniform. Far from the step, c_2 is constant at 0.40 ML, but near the step it decreases to half that value. One possibility is that surface diffusion is inhibited (e.g., when c_3 is large) and that c_2 is not equilibrated laterally. An alternative scenario is that the c_2 is equilibrated and that the variation in c_2 with c_3 is due to a repulsive Pd-Pd interaction. In this case, the correlation between c_2 and c_3 can be used to infer the strength of this interaction. For example, if there were no interaction between Pd atoms, then c_2 would be spatially uniform, and there would be no correlation with c_3. Alternatively, if Pd atoms strongly repel, then c_2 will be small when c_3 is large, and vice versa. Consider a highly simplified model in which the internal energy of the film is proportional to the number of Cu-Pd nearest-neighbor (NN) bonds. This model is motivated by the stability of the $c(2 \times 2)$ structure, in which *all* of the Pd NNs are Cu, and is supported by first-principles calculations [13] as well as empirical modeling [14]. The theoretical analysis of the bonding shows that Cu-Pd NN bonds are favored over both Cu-Cu and Pd-Pd bonds.

We performed Monte Carlo simulations on the model outlined above to determine if the measured correlation between c_2 and c_3 is consistent with a fully equilibrated second layer. We do this by computing the equilibrium alloy concentrations for a given value of the Cu-Pd NN bond energy ϵ and comparing to the measured concentration profiles shown in Fig. 4(a) (taking all other bond energies to be zero). In the simulations, we used the Metropolis algorithm [15] to compute c_1 and c_2 given a fixed distribution of Pd in the third layer [16]. The two free parameters of the model are ϵ and the Pd chemical potential μ [17]. Details of the simulations are given elsewhere [12]. We fix the two model parameters to match the experimental result far from the step: $c_1 \approx 0.05$ and $c_2 \approx 0.40$. We then compute c_1 and c_2 as a function of c_3, which is taken from the measured profile. The black curves in Fig. 4(a) show the simulation results for $\epsilon = -25$ meV. The agreement is remarkable given the simplicity of the model. The ability to quantitatively reproduce the measured composition profile strongly suggests that the first two layers are, in fact, laterally equilibrated. That is, the decrease in c_2 in the overgrown region near the step reflects an effective Pd-Pd repulsion rather than slow Pd diffusion at the surface. These results also explain how inhomogeneity in the third layer is propagated into the second layer: c_2 and c_3 are highly correlated. The correlation is driven by the effective repulsion between Pd atoms.

Understanding compositional heterogeneity is a key challenge in the engineering of thin films. By carefully measuring how heterogeneity develops near steps, we have identified the exact process—step overgrowth coupled with inhibited bulk diffusion—that gives rise to heterogeneity. This mechanism is a direct consequence of the energetics of vacancy diffusion and is expected to be relevant in a wide range of growth systems. Proving that the step-overgrowth mechanism is operative in the absence of direct measurements of the concentration profiles is essentially impossible. However, our analysis shows that spatially resolved LEED analysis is a powerful method for determining three-dimensional alloy concentrations locally at surfaces with nanometer-scale resolution. Knowledge of how composition evolves in space and time places strict constraints on models of film equilibration, structure, stability, and growth.

*Electronic address: jbhannon@us.ibm.com
[1] E. Bauer, Rep. Prog. Phys. **57**, 895 (1994).
[2] R. R. Bourassa and B. Lengeler, J. Phys. F **6**, 1405 (1976).
[3] C. Klünker, J. B. Hannon, M. Giesen, H. Ibach, G. Boisvert, and L. J. Lewis, Phys. Rev. B **58**, R7556 (1998).
[4] J. B. Pendry, *Low Energy Electron Diffraction* (Academic, London, 1974).
[5] A. K. Schmid, W. Święch, C. S. Rastomjee, B. Rausenberger, W. Engel, E. Zeitler, and A. M. Bradshaw, Surf. Sci. **331–333**, 225 (1995).
[6] F. Jona, K. O. Legg, H. D. Shih, D. W. Jepsen, and P. M. Marcus, Phys. Rev. Lett. **40**, 1466 (1978).
[7] C. J. Barnes, E. AlShamaileh, T. Pitkänen, P. Kaukasoina, and M. Lindroos, Surf. Sci. **492**, 55 (2001).
[8] H. L. Davis and J. R. Noonan, J. Vac. Sci. Technol. **20**, 842 (1982).
[9] J. Rundgren, Phys. Rev. B **59**, 5106 (1999).
[10] S. Müller, A. Kinne, M. Kottcke, R. Metzler, P. Bayer, L. Hammer, and K. Heinz, Phys. Rev. Lett. **75**, 2859 (1995).
[11] S. Walter, V. Blum, L. Hammer, S. Müller, K. Heinz, and M. Giesen, Surf. Sci. **458**, 155 (2000).
[12] J. Sun, J. B. Hannon, G. L. Kellogg, and K. Pohl (to be published).
[13] J. Kudrnovský, S. K. Bose, and V. Drchal, Phys. Rev. Lett. **69**, 308 (1992).
[14] J. B. Hannon, H. Ibach, and P. Stoltze, Surf. Sci. **355**, 63 (1996).
[15] N. Metropolis, A. W. Rosenbluth, M. N. Rosenbluth, A. H. Teller, and E. Teller, J. Phys. Chem. **21**, 1087 (1953).
[16] A trial move in the simulation involves swapping the identities of two atoms in the top two layers of the film.
[17] To be precise, the chemical potential in the model is the energy to replace a Cu atom in one of the first two layers with a Pd atom. The value simply sets the total Pd concentration of the film.